Proceedings of the 2001 IEEE
International Conference on Robotics & Automation
Seoul, Korea • May 21-26, 2001

Design Of A New 6-DOF Parallel Haptic Device

J. H. Lee, K. S. Eom, B-J Yi, I. H. Suh

School of Electrical Engineering and Computer Science, Hanyang University, Korea

Email : bj@email.hanyang.ac.kr

Abstract *In this paper, a new 6-dof parallel haptic master device is proposed. Many existing haptic devices require large power due to having floating actuator and also have small workspaces. The proposed new mechanism is relatively light by employing non-floating actuators and has large workspace. Kinematic analysis and kinematic optimal design problem is performed for this mechanism. Dexterous workspace, global isotropic index, and global maximum force transmission ratio are considered as kinematic design indices. To deal with such multi-criteria optimization problem, composite design index is employed. Actuator sizing for this mechanism is also carried out.*

Keywords : Haptic Device, Parallel Mechanism, Optimal Design

1. Introduction

The application of virtual reality is expanding fast in various areas: medical, teleoperation, entertainment, etc. Virtual reality technology mainly consists of vision, haptic display, and audio. However, progress in the field of haptic interface has been much slower than vision and audio, relatively.

Since master-slave system proposed by Goertz in the 1950's[1], many researchers have developed various type of haptic display such as an exoskeleton type master arm by M. Bergamasco[5], PHANToM[3] by Massie and Salisbury, MagLev Wrist[4] by Hollis in Carnegie Mellon Univ., and the magnetic levitation haptic interface by Merkelman et al, etc. Although many haptic interfaces have been developed as above, they have generally three or less DOF which are not enough to display the real phenomenon. And they mostly have serial structures which can not achieve hard contact feeling. Other devices having parallel structure are heavy and have relatively small workspace, and required large power due to floating actuators[2,6,8].

General requirements of Haptic interface include large workspace for human operator, low apparent mass/inertia, low friction, high structural stiffness, backdriveability, low backlash, high force bandwidth, high force dynamic range, absence of mechanical singularities, compactness, an even 'feel' through the workspace, and so on[2]. These requirements can be fulfilled by employing a good mechanism in company with good control algorithm.

In this paper, we will propose a new 6-DOF parallel haptic interface which is actuated by non-floating actuators as shown in Fig. 1. This new mechanism has large workspace with no singularity. To maximize kinematic performances of the haptic interface, multi-criteria based optimization is carried out.

2. Kinematics of a new 6-DOF Haptic Device

2.1 Geometric Description

The proposed 6-DOF Haptic Device consists of a top plate, six actuators on the base, and three parallel chains connecting the top plate to the six actuators in Fig. 2. Let $\{B\}$ and $\{T\}$ be the base frame fixed to the ground with its origin at the center of the base and the local frame fixed to the top plate with its origin at the center of the top frame, respectively. Each of three ball-socket joints (${}^{m}\underline{C}$, $m=1,2,3$) of the top plate are placed on the circle of radius (R_t) with 120° apart from each other. Three pairs of actuators are placed on the ground with 120° apart from each other. Each of three actuator pairs consists of the upper actuator (M1) that is placed on the circle of radius R_{B1} horizontal to the ground and the lower actuator (M2) that is placed on the circle of radius R_{B2} vertical to the ground. And H_B denotes the distance from upper actuator and lower actuator in the x-direction.

Each chain consists of upper closed-chain and lower closed-chain as Fig. 3. The upper chains connect the ball-socket joint (${}^{m}\underline{C}$, $m=1,2,3$) of the top plate to the upper actuator (M1).

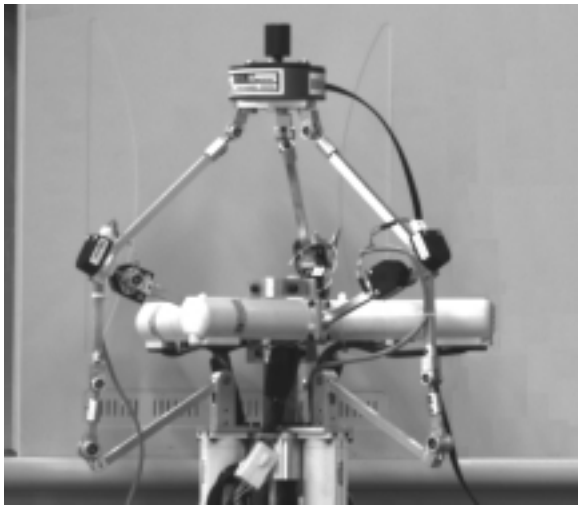

Fig. 1. New 6-DOF Parallel Haptic Device

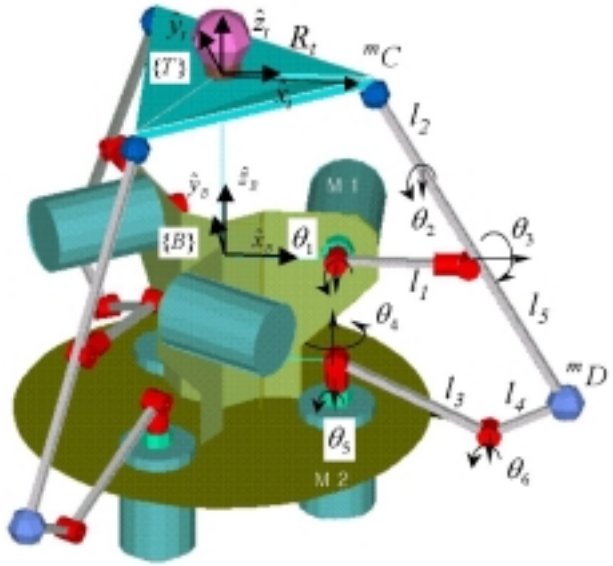

Fig. 2 Kinematic Structure of New 6 DOF Haptic Device

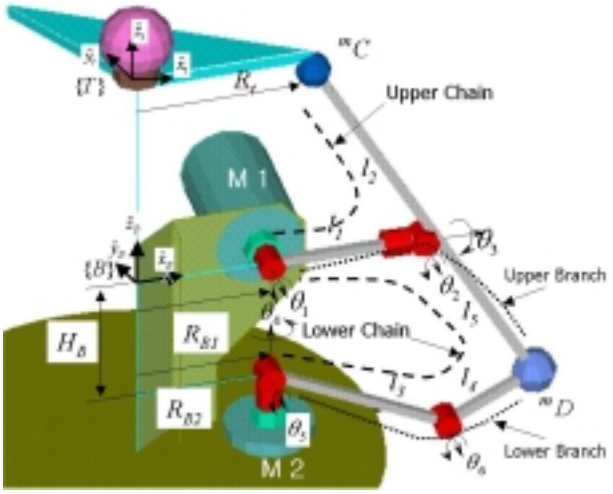

Fig. 3 Leg Structure of 6 DOF Parallel Haptic Device

And the lower chains connect the lower ball-socket joint (${}^{m}\underline{D}$, $m=1,2,3$) to the lower actuator (M2). So upper actuators support gravity loads and generate the z-directional motion, and the lower actuators generate x-, and y-directional motions, respectively. Interaction of the three chains generates the Rotational motion.

We define the output displacement vector as

$$\underline{u}=(x_t, y_t, z_t, \theta_x, \theta_y, \theta_z)^T, \quad (1)$$

where (x_t , y_t , z_t) represent the positions of the origin of the top plate, and (θ_x , θ_y , θ_z) denotes $\hat{x}_t$ - $\hat{y}_t$ - $\hat{z}_t$ Euler angles equivalent to $[R_b^t]$ expressed by

$$[R_b^t]=[Rot(\hat{x}_t,\theta_x)]\,[Rot(\hat{y}_t,\theta_y)]\,[Rot(\hat{z}_t,\theta_z)] \quad . \quad (2)$$

2.2 Forward Kinematics

General parallel mechanisms have many forward kinematic solutions, and this new 6-DOF parallel haptic device has 8-th order polynomial. So we place 3 additional encoders at passive joints(θ_2) of upper chains to obtain a unique forward solution.

2.3 Inverse Kinematics

We can solve the inverse kinematic solution of each upper chain from the position vectors of the upper ball-socket joint (${}^{m}\underline{C}$), which are given from the position and orientation of the top plate. In the same manner, the inverse kinematic solution of each lower chain can be obtained from position vectors of the lower ball-socket joint (${}^{m}\underline{D}$, $m=1,2,3.$), which are given from the forward kinematics of the upper chain.

2.4 First-order Kinematic Modeling

In the following, we describe the 1-*st* order KIC (Kinematic Influence Coefficient) as the relationship between the operational velocity ($\dot{\underline{u}}$) and the active joint velocity ($\dot{\underline{\theta}}_A$). Three upper contact points located at the upper ball-socket joints are denoted as

$$\underline{C}=({}^{1}\underline{C}^T, {}^{2}\underline{C}^T, {}^{3}\underline{C}^T)^T, \quad (3)$$

where

$${}^{m}\underline{C}=({}^{m}_{c}x, {}^{m}_{c}y, {}^{m}_{c}z)^T. \quad (4)$$

Each upper contact point vector is expressed as

$${}^{m}\underline{C}=\underline{u}_t+{}^{m}_{c}\underline{r}, \quad (5)$$

where

$${}^{m}_{c}\underline{r}=[R_b^t]\;{}^{m}_{c}\underline{r}^{(t)}. \quad (6)$$

Differentiating ${}^{m}\underline{C}$ with respect to time results in

$${}^{m}\dot{\underline{C}}=\dot{\underline{u}}_t+\underline{\omega}\times{}^{m}_{c}\underline{r}, \quad (7)$$

where

$$\dot{\underline{u}}_t=(\dot{x}_t, \dot{y}_t, \dot{z}_t)^T, \quad (8)$$

$$\underline{\omega}=(\omega_x, \omega_y, \omega_z)^T, \quad (9)$$

and

$${}^{m}_{c}\underline{r}=({}^{m}_{c}r_x, {}^{m}_{c}r_y, {}^{m}_{c}r_z)^T. \quad (10)$$

Eq. (7) can be written in a matrix form as

$${}^{m}\dot{\underline{C}}=[{}^{m}G_u^c]\;\dot{\underline{u}}, \quad (11)$$

where

$$[{}^{m}G_u^c]=\begin{bmatrix}1&0&0&0&{}^{m}_{c}r_z&-{}^{m}_{c}r_y\\0&1&0&-{}^{m}_{c}r_z&0&{}^{m}_{c}r_x\\0&0&1&{}^{m}_{c}r_y&-{}^{m}_{c}r_x&0\end{bmatrix}, \quad (12)$$

$$\dot{\underline{u}}=(\dot{x}_t, \dot{y}_t, \dot{z}_t, \omega_x, \omega_y, \omega_z)^T. \quad (13)$$

Then the relationship between $\dot{\underline{u}}$ and $\dot{\underline{C}}$ can be described as

$$\dot{\underline{C}}=[G_u^c]\dot{\underline{u}}, \quad (14)$$

where

$$[G_u^c] = \left[\; [{}^1G_u^c]^T [{}^2G_u^c]^T [{}^3G_u^c]^T \right]^T . \quad (15)$$

The open-chain kinematics of each leg is described as

$${}^m\dot{\underline{C}} = [{}^m_u G_\theta^c] \; {}^m_u\dot{\underline{\theta}}, \quad (16)$$

where ${}^m_u\dot{\underline{\theta}}$ is the velocity vector of the joints in m-*th* upper chain.

Assuming no singularity in $[{}^m_u G_\theta^c]$, the first-order inverse kinematic formulation is obtained as

$${}^m_u\dot{\underline{\theta}} = [{}^m_u G_c^\theta] \; {}^m\dot{\underline{C}} . \quad (17)$$

Congregating from $m = 1$ to 3 yields

$${}_u\dot{\underline{\theta}} = [{}_u G_c^\theta] \; \dot{\underline{C}} . \quad (18)$$

where

$${}_u\dot{\underline{\theta}} = ({}^1_u\dot{\underline{\theta}}^T \quad {}^2_u\dot{\underline{\theta}}^T \quad {}^3_u\dot{\underline{\theta}}^T)^T ,$$

and

$$[{}_u G_c^\theta] = \begin{bmatrix} [{}^1_u G_c^\theta] & 0 & 0 \\ 0 & [{}^2_u G_c^\theta] & 0 \\ 0 & 0 & [{}^3_u G_c^\theta] \end{bmatrix} .$$

2.5 Internal Kinematics

The lower closed chain consists of two branches which are constrained by the lower ball-socket joint (${}^m\underline{D}$, $m = 1 \sim 3$), and the common velocity is described as

$${}^m\dot{\underline{D}} = [{}^m G_{u\theta}^D] \; {}^m_u\dot{\underline{\theta}} = [{}^m G_{l\theta}^D] \; {}^m_l\dot{\underline{\theta}} \quad , \quad (19)$$

where $[{}^m G_{u\theta}^D]$ and $[{}^m G_{l\theta}^D]$ represent the 1-*st* order KICs for the upper branch and the lower branch, respectively. From Eq. (18), we can obtain the first-order kinematic relationship between the upper branch and the lower branch as

$${}^m_l\dot{\underline{\theta}} = [{}^m G_{l\theta}^D]^{-1} [{}^m G_{u\theta}^D] \; {}^m_u\dot{\underline{\theta}} = [{}^m G_{u\theta}^{l\theta}] \; {}^m_u\dot{\underline{\theta}}, \; m = 1 \sim 3 . \quad (20)$$

By using a row-column selection of Eq. (20), the first-order relationship between the active joint velocity(${}^m\dot{\underline{\theta}}_A$: ${}^m\dot{\theta}_1$, ${}^m\dot{\theta}_4$, $m = 1 \sim 3$) and the joint velocity(${}_u\dot{\underline{\theta}}$) of the upper chains can be expressed as

$$\dot{\underline{\theta}}_A = [G_{u\theta}^A] \; {}_u\dot{\underline{\theta}}, \quad (21)$$

where

$$[G_{u\theta}^A] = \begin{bmatrix} 1 & 0 & 0 & \underline{0} & \underline{0} \\ [{}^1G_{u\theta}^{l\theta}]_{1;} & & & \underline{0} & \underline{0} \\ \underline{0} & 1 & 0 & 0 & \underline{0} \\ \underline{0} & [{}^2G_{u\theta}^{l\theta}]_{1;} & & & \underline{0} \\ \underline{0} & \underline{0} & & 1 \; 0 \; 0 & \\ \underline{0} & \underline{0} & & [{}^3G_{u\theta}^{l\theta}]_{1;} & \end{bmatrix}_{(6\times 9)} , \quad (22)$$

$${}_u\dot{\underline{\theta}} = [{}^1\theta_1 \; {}^1\theta_2 \; {}^1\theta_3 \; {}^2\theta_1 \; {}^2\theta_2 \; {}^2\theta_3 \; {}^3\theta_1 \; {}^3\theta_2 \; {}^3\theta_3]^T_{(9\times 1)} . \quad (23)$$

Substituting Eq. (17) into Eq. (21) yields the following relationship between the velocity of upper contact point the active joint velocity

$$\dot{\underline{\theta}}_A = [G_c^A] \; \dot{\underline{C}} \quad , \quad (24)$$

where

$$[G_c^A] = [G_{u\theta}^A][{}_u G_c^\theta] . \quad (25)$$

And by substituting Eq. (14) into Eq. (24), the relationship between the operational velocity and active joint velocity is obtained as

$$\dot{\underline{\theta}}_A = [G_u^A] \; \dot{\underline{u}} \quad (26)$$

where

$$[G_u^A] = [G_c^A][G_u^c] . \quad (27)$$

Assuming no singularity in $[G_u^A]$, the forward Jacobian is obtained by matrix inversion as

$$\dot{\underline{u}} = [G_A^u] \; \dot{\underline{\theta}}_A . \quad (28)$$

2.6 Jacobian Scaling

General spatial motion involves both the translation and the rotation. Therefore, the Jacobian for this case has different units in the translational part and the rotational part. When the translational motion and the rotational motion are investigated separately, the result does not represent general 6-DOF motion characteristics. Many scaling techniques to treat the translational and rotational parts simultaneously have been proposed[9]. In this work, a Jacobian scaling technique based on the nominal link(l_{NL}) whose length is defined as the distance from the origin of the base frame to the midpoint of the top plate, is employed.

The scaled form of the Jacobian is related to the original jacobian as

$$[{}^*G_A^u] = [S][G_A^u], \quad (29)$$

where

$$[S] = \begin{bmatrix} [I] & \underline{0} \\ \underline{0} & [l_{NL}]_{diag} \end{bmatrix} . \quad (30)$$

3. Kinematic Design Performance Index

Many aspects can be considered in the design of haptic device. Workspace, kinematic isotropy, and force transmission ratio are considered in this paper. Workspace means operating space for human operator, kinematic isotropy is a criteria which indicate how evenly the system moves in all directions. And force transmission ratio is also important to save input energy.

3.1 Workspace

One of the basic aspects of haptic device design is determining the workspace. The operating region or workspace of a manipulator is defined as a reachable and dexterous workspace. Also, a manipulator should be designed for the workspace property of well-connectedness, while allowing its end-effector to move from one regular point to another without passing through a critical value(i.e., singularity). A larger workspace enables the user to work in a wide range. This implies that this index should be maximized. The workspace volume is defined as

$$V = \int_V dV \,, \tag{31}$$

where the orientation angle of the top plate is defined as

$$-45^\circ \le \theta_x, \theta_y \le 45^\circ \,,\ -90^\circ \le \theta_z \le 90^\circ \,. \tag{32}$$

3.2 Kinematic Isotropic Index

The Kinematic Isotropic Index is defined as

$$\sigma_I = \frac{\sigma_{\min}(*[G_A^u])}{\sigma_{\max}(*[G_A^u])} \,. \tag{33}$$

where $\sigma_{\min}$ and $\sigma_{\max}$ denote the minimum and the maximum singular values of $*[G_A^u]$, respectively. When σ_I approaches unity, the end-effector can generate uniform velocity in all directions. Also, global design index which represents the average of the manipulator's isotropic index over the whole workspace is defined as

$$\Sigma_I = \frac{\int_V \sigma_I dV}{\int_V dV} \,. \tag{34}$$

The greater Σ_I is, the better isotropy the mechanism has over the workspace. Therefore, Σ_I should be maximized.

3.3 Maximum Force Transmission Ratio

The maximum force transmission ratio implies the maximum magnitude of an actuator load required for the unit end-effector force, and it is defined as

$$\sigma_F = \sigma_{\max}([*G_A^u]) \,. \tag{35}$$

If σ_F becomes smaller, the actuator load will be reduced. This means that the manipulator can bear more weight with less actuators. The global design index for σ_F is defined as

$$\Sigma_F = \frac{\int_V \sigma_F dV}{\int_V dV} \,. \tag{36}$$

The smaller Σ_F is, the smaller capacity of the actuator is required. Thus, Σ_F should be minimized.

4. Optimum Design

In order to maximize the performances of the proposed haptic device, multi-criteria based design methodology based on genetic optimization algorithm are employed.

4.1 Composite Design Index(Cost function)

Several methodologies have been proposed to cope with multi-criteria based design. However various design indices are usually incommensurate concepts due to differences in unit and physical meanings, and therefore should not be combined unless they are transferred into a common domain. In consideration of this fact, a multi-criteria based design methodology employing a concept of composite design index is introduced[10]. This process consist of normalization which transfer various indices into a same domain and synthesis which combines several indices into one.

For V and Σ_I, the most favored preference is given the maximum value, and the least favored preference is given the minimum value of the criterion. Then, the preference design indices, $\tilde{V}$ and $\tilde{\Sigma}_I$ are expressed as

$$\tilde{V} = \frac{V - V_{min}}{V_{max} - V_{min}} \,, \tag{37}$$

$$\tilde{\Sigma}_{KSI} = \frac{\Sigma_{KSI} - (\Sigma_{KSI})_{min}}{(\Sigma_{KSI})_{max} - (\Sigma_{KSI})_{min}} \,, \tag{38}$$

where, "~" on each design index implies that it is transferred into the common preference design domain. Conversely, for $\tilde{\Sigma}_F$, the top preference is given the maximum value of the criterion. Then, the preference design indices , $\tilde{\Sigma}_F$ is expressed as

$$\tilde{\Sigma}_F = \frac{(\Sigma_F)_{\max} - \Sigma_F}{(\Sigma_F)_{max} - (\Sigma_F)_{min}} \,. \tag{39}$$

To deal with this multi-criteria based design, a kinematic composite design index(KCDI) is employed which combines several individual preference design indices as a unique design index by using the max-min principle of fuzzy theory. KCDI is expressed as

$$KCDI = \min\{\tilde{V},\ \tilde{\Sigma}_{KSI},\ \tilde{\Sigma}_F\} \,. \tag{40}$$

KCDI is defined as the minimum value among the preference design indices calculated for a set of kinematic parameters. And a set of design parameters, which has the maximum value of the KCDI, is chosen as the optimal set of design parameters.

Table 1 Kinematic Constraint

Constant Parameters (mm)							
Motor Diameter		R_{B1}		$l_1 + l_2$			
50		50		250			
Variable Parameters (mm)							
l_2		l_3		l_4		l_5	
Min.	Max.	Min.	Max.	Min.	Max.	Min.	Max.
30	220	30	150	30	130	30	130
R_t		R_{B2}		H_B			
Min.	Max.	Min.	Max.	Min.	Max.		
30	130	30	70	40	100		

4.2 Design Parameters and Constraint

The Kinematic design parameters for the new 6-dof haptic device are the radius of the top plate, R_t, the link lengths of each leg, l_1, l_2, l_3, l_4, l_5, and the horizontal distance(R_{B2}) and vertical distance(H_B) from the base origin to the lower actuator($M2$).

These design parameters and space constraints are described in Table 1. Motor diameter, R_{B1}, and the sum of l_1 and l_2 are set to some constant values to provide the

size limit of the whole system. And the other parameters are also bounded to guarantee the space of joint.

4.3 Optimization result

Genetic algorithm is employed to solve the nonlinear kinematic optimization for the new 6-DOF parallel haptic device[7]. We set the population size to 20. And in each generation we evaluate KCDI of each chromosome, select new population with respect to the probability distribution based on fitness values, and alter the chromosomes in the new population by mutation and crossover operators. After some number of generations, we obtain the best chromosome(parameter set) which represents an optimal solution. The optimization result is represented in Table 2. Figure 3 denotes the distribution of the kinematic indices resulting from optimization.

Table 2 Optimization Result

Design Parameters (mm)				
l_1	l_2	l_3	l_4	l_5
89.3	160.7	133.5	55.1	98.0
R_t	R_{B1}	R_{B2}	H_B	
37.7	50.0	50.0	50.0	
Performance				
Workspace (cm^3)	Average Kinematic Isotropy	Average Force Transmission Ratio		
1010.0	0.0158	0.00225		

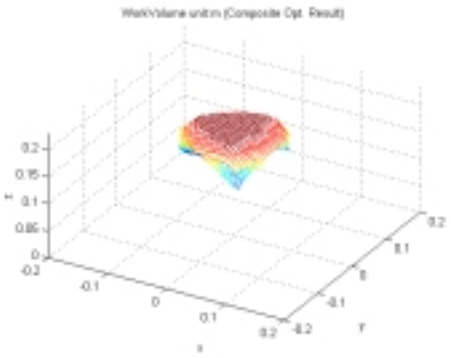

(a) Dexterous Workspace

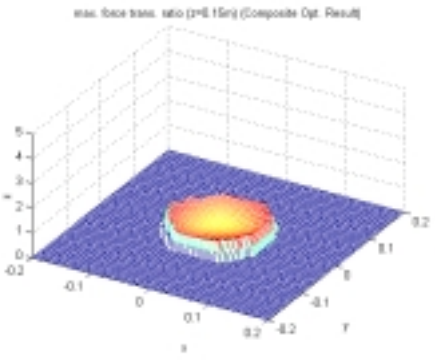

(b) Force Transmission Ratio

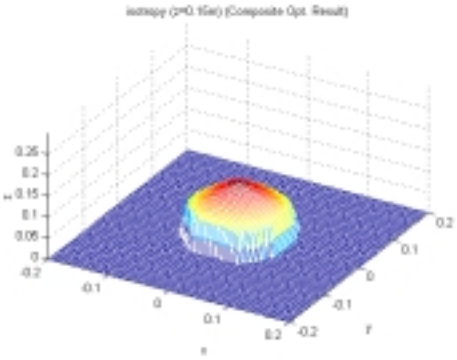

(c) Kinematic Isotropy

Fig. 4. Distribution of Performance Indices

4.4 Tolerance Analysis

General manipulators have inevitable joint tolerance due to manufacturing bottleneck. This tolerance causes undesirable motion or curtails performance, and thus we have to consider the design which minimizes its effect.

To analyze the effect of tolerance on the upper plate, most severe joints causing undesirable displacement have to be identified. For the designed device, the tolerance of the joint 4 of each chain is notable. Thus a Jacobian relating the output to the three pseudo-joints is expressed as

$$\delta \underline{u} = [G_{\theta_t}^{u}]\ \delta \underline{\theta}_t . \qquad (41)$$

The displacement of upper plate due to tolerance at joint 4 is displayed in Fig. 6. In this example, the error range of the joint tolerance is $\pm 0.5^\circ$, and the initial position of the upper plate is $u = [0 \quad 0 \quad 0.5]^T$. To minimize this tolerance effect, a design index representing the size of the tolerance effect should be incorporated into the optimization problem.

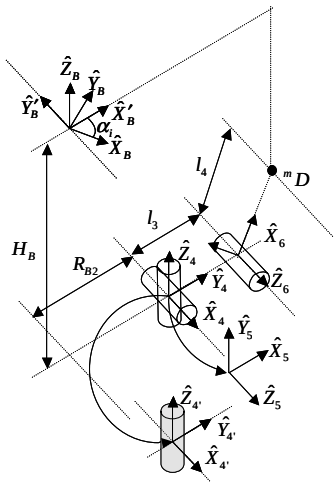

Fig. 5. Coordinate Including Joint with Tolerance

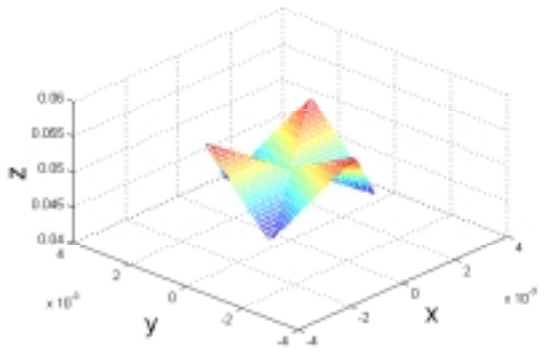

Fig. 6. Errors in Upper Coordinate by Joints with Tolerance

5. Actuator Sizing

Actuator size is defined as maximum joint torque enough to withstand the given external load and gravity, and can be computed as following[11].

The output load is bound as

$$T_u = \left\| \underline{T}_u \right\|_2 = (\underline{T}_u [W] \underline{T}_u)^{1/2} \le (T_u)_{\max}, \quad (42)$$

with $(\theta_i)_{\min} \le \theta_i \le (\theta_i)_{\max}, \ i = 1, 2, \cdots, N_p$ (43)

where $(T_u)_{\max}$ is the maximum external load, θ_i is the angle of the i-th joint, and N_p is the number of all joints. The actuator torque due to the external load is expressed as

$$(T_{An})_{ext} = (T_u)_{\max} ([G_A^u]_{;n}^T [W]^{-1} [G_A^u]_{;n})^{\frac{1}{2}}. \quad (44)$$

Consequently, the required torque at the n-th actuator is the sum of $(T_{An})_{ext}$ supporting the external load and T_{An}^G supporting the gravity load as

$$T_{An}^M = \max \left\{ \left| T_{An}^G + (T_{An})_{ext} \right|, \left| T_{An}^G - (T_{An})_{ext} \right| \right\}. \quad (45)$$

The maximum T_{An}^M for the entire workspace is the appropriate actuator size. To generate the force of $20\,N$ and the torque of $1.0\,Nm$ at the end effector, the actuator sizes are calculated as in Table 3.

Table 3. Actuator Size

Payoad at the top plate	Actuator Torq.(Nm)	
Force(20.0 N)	T_{A1}	2.88
	T_{A2}	12.03
Torq.(1.0 Nm)	T_{A1}	3.79
	T_{A2}	6.79
Force(20.0 N) + Torq.(1.0 Nm)	T_{A1}	4.53
	T_{A2}	13.82

6. Conclusion

A new 6-dof parallel haptic device which is actuated by non-floating actuators is proposed. This device is adequate for haptic device due to light weight and high force-reflecting capability. To design the haptic mechanism, a multi-criteria based kinematic optimal design problem is formulated, which simultaneously considers various indices. And the optimal solution is found by employing Genetic Algorithm. Actuator sizing is also carried out to complete the design problem. More sophisticated design minimizing the loss of position accuracy due to the joint clearance has to be further studied. And application of the purposed haptic device to manipulation of virtual reality is ongoing subject.

Acknowledgement

This work was supported by grant No. (2000-2-30200-008-3) from the Basic Research Program of the Korea Science & Engineering Foundation.

Reference

[1] R.C. Goertz, “Fundamentals of General-Purpose Remote Manipulators,” Journal of Nucleonics, Vol. 10, No. 11, pp.36-42, 1952.

[2] R.E. Ellis, O.M. Ismaeil, and M.G. Lipsett, “Design and Evaluation of High-Performance Haptic Interface”, Robotica, Vol.4., 1996.

[3] T. Massie, K. Stalisbury, "PHANToM Haptic Interface: A Device for Probing Virtual Objects", ASME Journal of Dynamic System and Control, New York, NY, pp.295-299, 1994.

[4] P. J. Berkelman, R. L. Hollis, and S. E. Salcudean, "Interacting with Virtual Environments using a Magnetic Levitation Haptic Interface", Proceedings of IEEE International Conference on Intelligent Robots and Systems, pp. 117-122, piscataway, NJ, 1995.

[5] M. Bergamasco, et al., “An Arm Exoskeleton System for Teleoperation and Virtual Environments Applications,” Proceedings of International Conference On Robotics and Automation, San Diego, California, pp. 1449-1454, 1994.

[6] M. Ishii and M. Sato, “A 3D Spatial Interface Device Using Tensed Strings,” Presence-Teleoperators and Virtual Environments, Vol.3, No.1, MIT Press, Cambridge, MA, pp.81-86, 1994.

[7] Zbigniew Michalewicz, “Genetic Algorithms + Data Structures = Evolution Programs,” Springer, 1996.

[8] J.M. Hollerbarch, “Some Current Issues in Haptic Research,” Proceedings of International Conference On Robotics and Automation, pp. 757-762, 2000.

[9] Leo J. Stocco, S. E. Salcudean, and F. Sassani, “On the Use of Scaling Matrices for Task-Specific Robot Design”, IEEE Transactions On Robotics And Automation, Vol. 15, No. 5, October 1999.

[10] J.H. Lee, B-J. Yi and S.R. Oh, “Optimal Design of a Five-Bar Finger with Redundant Actuation,” Proceedings of International Conference On Robotics and Automation, pp. 2068-2074, 1998.

[11] M. Thomas, H.C. Yuan-Chou, and D. Tesar, “Optimal Actuator Sizing for Robotic Manipulators Based on Local Dynamic Criteria,” ASME Journal of Mechanisms, Transmissions and Automation in Design, Vol. 107, pp.163-169, 1985.